Toward a Systematic Understanding of Photodetectors Based on Individual Metal Oxide Nanowires

ARTICLE *in* THE JOURNAL OF PHYSICAL CHEMISTRY C · SEPTEMBER 2008

Impact Factor: 4.77 · DOI: 10.1021/jp804614q

THE JOURNAL OF PHYSICAL CHEMISTRY C

Article

Toward a Systematic Understanding of Photodetectors Based on Individual Metal Oxide Nanowires

Joan Daniel Prades, Roman Jimenez-Diaz, Francisco Hernandez-Ramirez, Luis Fernandez-Romero, Teresa Andreu, Albert Cirera, Albert Romano-Rodriguez, Albert Cornet, Joan Ramon Morante, Sven Barth, and Sanjay Mathur

J. Phys. Chem. C, **2008**, 112 (37), 14639-14644• DOI: 10.1021/jp804614q • Publication Date (Web): 22 August 2008

Toward a Systematic Understanding of Photodetectors Based on Individual Metal Oxide Nanowires

Joan Daniel Prades,*,† Roman Jimenez-Diaz,† Francisco Hernandez-Ramirez, Luis Fernandez-Romero,† Teresa Andreu,† Albert Cirera,† Albert Romano-Rodriguez,† Albert Cornet,† Joan Ramon Morante,† Sven Barth,‡ and Sanjay Mathur*,‡,§

EME/XaRMAE/IN²UB, Departament d'Electronica, Universitat de Barcelona, C/ Marti i Franques 1, Barcelona, E-08028, Spain, Nanocrystalline Materials and Thin Film Systems, Leibniz-Institute of New Materials, Saarbruecken, D-66123, Germany, and Department of Inorganic Chemistry, University of Cologne, Cologne, D-50939, Germany

Received: May 20, 2008; Revised Manuscript Received: July 3, 2008

We present a set of criteria to optimize photodetectors based on n-type metal oxide nanowires and a comparison methodology capable of overcoming the present lack of systematic studies dealing with such devices. The response of photoconductors is enhanced following different fabrication strategies, such as diminishing the distance between the electrical contacts, increasing the width of the photoactive area, or improving the electrical mobility of the nanomaterials. The validity of the theoretical background is verified by experimental results obtained with devices based on ZnO nanowires. The performances of our devices show that the normalized gain of single ZnO nanowire-based photodetectors exceeds those of thin films.

Introduction

Metal oxide nanowires are gaining growing interest as photodetectors due to their potential applications in gas sensing and optoelectronics.[1] Although preliminary works revealed promising results,[1−11] further research is necessary in order to reach complete control of their photosensing properties. Among all n-type metal oxide nanomaterials, photoresponses of ZnO and SnO_2 nanowires have been widely studied;[1−11] however, the lack of well-established fabrication methodologies and standardized procedures obfuscates a comparison of experimental results. For instance, photoconductive gains (G_{ph}) ranging from 10^2 to 10^8 [4,9,10] and response times (τ) between milliseconds and hours were reported for ZnO nanowires,[1,2,4,7,10] which possibly result from different experimental conditions and device geometry used in all of these studies. Here, we present some systematic strategies for enhancing the response of photodetectors based on nanowires and a methodology for the facile comparison of the measured photoresponses. These strategies are fundamental to the potential of this technology in real devices and applications.

Experimental Methods

ZnO nanowires were fabricated via a vapor-phase carbothermal transport process inside an Atomate's chemical vapor deposition (CVD) system. The source material was a 1:1 molar mixture of commercial ZnO (metal basis, 99.99%) and graphite powder (crystalline, 300 mesh, 99%) from Alfa Aesar. Gold nanoparticles were used as catalytic islands on thermally oxidized Si wafers.[12] Uniform nanowires were obtained with mean radius $<r> = 90 \pm 15$ nm and lengths up to 30 μm. Some of them were electrically contacted to platinum microelectrodes using a FEI Dual-Beam Strata 235 FIB instrument following a nanolithography process explained elsewhere.[13−15] Electrical measurements were performed with the help of a self-made electronic circuit designed to ensure low current levels and to avoid undesired fluctuations[16] inside a homemade chamber. Photoresponse was excited using both UV LEDs and a UV lamp. UV LEDs were centered on $\lambda = 340 \pm 10$ nm and $\lambda = 385 \pm 15$ nm (Seoul Optodevices T9F34C and Purple-Hi E1L5M-4P0A2), whereas the UV lamp was a HAMAMATSU LC8 light source with a type[−01] Hg−Xe lamp enhanced for the line at $\lambda = 365$ nm. Light intensity impinging on the nanowires was determined with the help of a thermopile detector

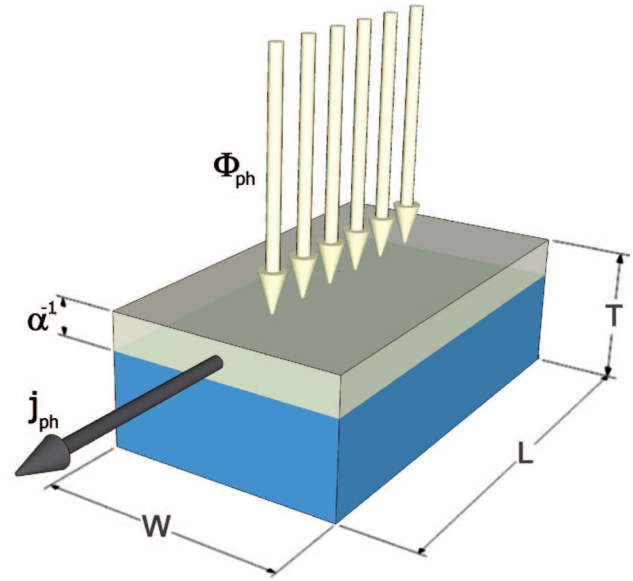

Figure 1. Diagram of a metal-oxide structure with an arbitrary volume of length L, width W, and thickness T, under a photon flux Φ_{ph}. Photocarrier generation is induced in the upper layer of the structure until a depth α^{-1} and leads to photoconduction (j_{ph}) under polarization.

* Corresponding authors: dprades@el.ub.es, s.mathur@uni-koeln.de.
† Universitat de Barcelona.
‡ Leibniz-Institute of New Materials.
§ University of Cologne.

10.1021/jp804614q CCC: $40.75
Published on Web 08/22/2008

(FieldMax-TOP). Up to 10 devices based on single ZnO nanowires were fabricated, and their photoresponses were studied as a function of different experimental parameters to validate the theoretical discussion. Two-probe I−V measurements revealed symmetric responses in great accordance with results published elsewhere.[17] The effective voltage drop along the nanowires was determined by decoupling the rectifying contact from the purely resistive contribution of the nanowires following the procedure described elsewhere.[17] To evaluate the role of surface contribution on the photoresesponse of these devices, some samples were coated with a 475 ± 50 nm thick layer of PMMA (2 wt % poly (methyl methacrylate) in dichloromethane) by spin coating. All experiments were performed in real air atmosphere.

Results and Discussion

1. Theoretical Background. Photodetectors based on single n-type metal oxide nanowires, modeled as an arbitrary volume of length L, width W, and thickness T (Figure 1), can be studied using the fundamental principles ruling light carrier generation on semiconductors.[18] Thus, current density j_{ph} is given by the following equation,

$$j_{ph} = q\Delta n_{ph} v \tag{1}$$

where q is the elemental charge, Δn_{ph} is the concentration of generated carriers, and v is their velocity. Δn_{ph} can be also written as shown in eq 2,

$$\Delta n_{ph} = \frac{\eta F}{V_{ph}}\tau \approx \frac{\eta F}{\alpha^{-1}WL}\tau \tag{2}$$

where η is the quantum efficiency of carrier generation by one photon, F is the absorption rate of photons, τ is the carrier lifetime, and V_{ph} is the photogeneration volume (Figure 1).

The approximation in eq 2 assumes a constant carrier generation profile until the depth α^{-1}, where α is the absorption coefficient of the metal oxide at one fixed wavelength (see the Supporting Information). Δn_{ph} and τ are also related through the following continuity equation,[18]

$$\frac{\partial \Delta n_{ph}}{\partial t} = g_{ph} - \frac{\Delta n_{ph}}{\tau} \tag{3}$$

where g_{ph} is the generation rate of charge carriers under illumination. Assuming that the concentration of electrons Δn_{ph} is independent of τ, the photocurrent dynamics at the rising (time constant τ_r) and falling (time constant τ_d) edges are given by (see Supporting Information),

$$i_{ph}(t) = I_{ph}(1 - e^{-t/\tau_r}) \tag{4}$$

$$i_{ph}(t) = I_{ph}e^{-t/\tau_d} \tag{5}$$

where I_{ph} is the photocurrent at the steady-state. However, if an external field E is applied parallel to the longitudinal axis of ohmic nanowires, then the velocity of carriers (v) can be expressed in terms of the applied voltage (V) using the following formula,

$$v = \mu * E = \frac{\mu * V}{L} \tag{6}$$

where μ^* is the effective carrier mobility. According to the Matthiessen's rule, μ^* can be divided into the bulk (μ_B) and surface (μ_S) contribution according to eq 7.[18]

$$\frac{1}{\mu^*} = \frac{1}{\mu_B} + \frac{1}{\mu_S} \tag{7}$$

The absorption rate of photons F when metal oxide nanowires are exposed to a flux of Φ_{ph} photons can be also expressed by eq 8,

$$F = \beta\Phi_{ph}WL \tag{8}$$

where β is the fraction of photons not reflected by the surface, and WL is the effective area of one nanowire (see Figure 1). Therefore, using eqs 2, 6, and 8, current density j_{ph} can be rewritten as eq 9

$$j_{ph} = q\frac{1}{L\alpha^{-1}}\beta\eta\tau\mu * V\Phi_{ph} \tag{9}$$

To evaluate the total photogenerated current I_{ph}, which is the experimental response of real devices, we assume that nanowires are thick enough to absorb all the incident photons. That is to say,

$$T \geq \alpha^{-1} \tag{10}$$

Therefore, it can be deduced that thinner nanowires ($T < \alpha^{-1}$) will lead to lower photoresponses. On the contrary, the use of thicker nanowires ($T \gg \alpha^{-1}$) will not imply a further signal enhancement. For instance, the penetration depth α^{-1} of near-UV photons (wavelength from 400 to 250 nm) in ZnO is almost constant at 50 nm.[19] Thus, ZnO nanowires with radii slightly above $r \approx 25$ nm should be used to maximize photoresponse to UV-light in this wavelength range.

If the constant absorption profile approximation is maintained, photocurrent I_{ph} in nanowires that satisfy eq10 is given by eq 11,

$$I_{ph} = j_{ph}(\alpha^{-1}W) = q\frac{W}{L}\beta\eta\tau\mu * V\Phi_{ph} \tag{11}$$

where three different contributions are clearly identified. The first one is related to geometric parameters of the device (W/L), the second one to the intrinsic properties of nanowires ($\beta\eta\tau\mu^*$) and the third one only depends on the experimental conditions ($V\Phi_{ph}$). The performance of these devices can be also analyzed in terms of their photoconductive gain G_{ph}, which is defined in eq 12,[18]

$$G_{ph} \equiv \frac{I_{ph}}{qF} \approx \frac{1}{L^2}\eta\tau\mu V \tag{12}$$

where identical types of contributions are involved.

2. Experimental Validation and Discussion. ***2.1. Geometrical Aspects.*** Concerning the geometry of photodetectors, eq 11 implies enhanced I_{ph} with increasing width (W) of the photoactive area. To verify this, the responses of single ZnO nanowires and lamellae were compared.[20] ZnO lamellae were randomly obtained during the synthesis process of ZnO nanowires when the density of catalytic gold nanoparticles is very high (Figure 2). Other authors have postulated that the origin of these structures could be related to variations of the oxygen concentration during synthesis.[20] ZnO lamellae presented thicknesses (T) comparable to the diameter of the nanowires ($2r \approx 220$ nm), but their widths (W) were up to 10 times larger, allowing us to confirm the enhancement of I_{ph} with increasing photoactive areas (Figure 2a). To compare the UV photosensing performances of individual ZnO nanowires with ZnO lamellae, identical conditions were used in all experiments ($\Phi_{ph} = 3.3 \times 10^{18}$ ph m^{-2}

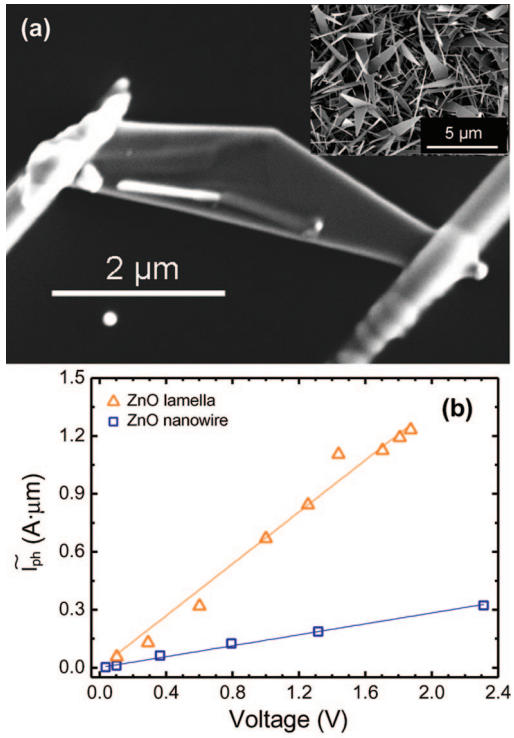

Figure 2. (a) ZnO lamella of length $L_L = 3.9\ \mu$m and average width around $W_L \approx 1000$ nm contacted with FIB nanolithography techniques. (Inset) SEM image of the mixture of ZnO nanowires and ZnO lamellae obtained after the synthesis process. (b) Normalized photoresponse $\tilde{I}_{ph}$ to the distance between electrical contacts L of one ZnO lamella and one ZnO nanowire ($L_{NW} = 13\ \mu$m) under identical conditions ($\Phi_{ph} = 3.3 \times 10^{18}$ ph m^{-2} s^{-1}; $\lambda = 340 \pm 10$ nm). I_{ph} is higher with the lamella due to a larger value of W.

s^{-1}; $\lambda = 340 \pm 10$ nm) and a comparable photocurrent ($\tilde{I}_{ph}$) value is obtained by normalization to the interelectrode distances (L).

$$\tilde{I}_{ph} = \frac{I_{ph}}{1/L} \tag{13}$$

The photoresponse [Figure 2] obtained with a nanowire was 4.7 times lower than the one measured with the lamella shown in Figure 2a. The average width of this lamellar structure was $W_L \approx 1000$ nm, whereas the nanowire showed $W_L \approx 220$ nm in diameter ($W_L/W_{NW} \approx 4.5$). In accordance to eq 11, the higher active area of ZnO lamellae caused enhanced photocurrent values $\tilde{I}_{ph}$ as predicted by geometrical factors and shown by the presented values ($W_L/W_{NW} \approx \tilde{I}_{ph(L)}\tilde{I}_{ph(NW)}$).

Another convenient way to increase the width of the photoactive area is using multi-nanowire-based configurations. These devices can be realized by self-assembly techniques, such as dielectrophoresis, to electrically contact large amounts of nanowires in parallel.[21,22] This fabrication methodology prevents parasitic effects arising from uncontrolled nanowire−nanowire contacts, and the resulting devices admit higher currents (with simpler conditioning electronics) without damaging the nanowires[16] (see the Supporting Information). It is noteworthy that, according to eq 12, the photoconductive gain G_{ph} obtained with these multi-nanowire configurations is equivalent to the gain provided by one single nanowire, if all of them are identical.

The distance between contacts (L) also determines the response of the photodetector since both I_{ph} and G_{ph} increase inversely with this parameter. L not only influences the photocapture area (WL) but also determines the effective electric

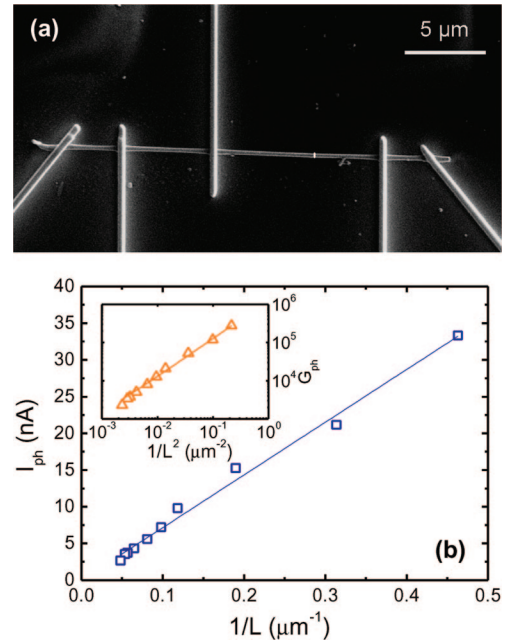

Figure 3. (a) ZnO nanowire with radius $r = 90 \pm 10$ nm contacted to five contacts fabricated with FIB nanolithography techniques. (b) Photoresponse I_{ph} and photoconductive gain G_{ph} (inset) of the ZnO nanowire as a function of the distance L between electrical contacts obtained with $\Phi_{ph} = 3.3 \times 10^{18}$ ph m^{-2}s^{-1}, $\lambda = 340 \pm 10$ nm, and $V = 1$ V.

field (E) inside the nanowire due to the bias voltage (V) applied externally. Indeed, this second aspect dominates the overall contribution of L to the photoresponse (see eqs 11 and 12). The dependence of I_{ph} and G_{ph} on L was experimentally confirmed by fabricating five electrical contacts separated at different distances on an individual ZnO nanowire (Figure 3a), and measuring the UV photoresponse between different pairs of electrodes. It was experimentally found that I_{ph} and G_{ph} increase inversely with the distance between contacts L, in accordance with eqs 11 and 12 (Figure 3b). Therefore, it can be concluded that higher-gain photodetectors are obtained by diminishing this fabrication-related parameter. The lower limit for L will strictly depend on the precision of the nanolithography technique and other size-associated phenomena such as diffraction, if L approaches the wavelength of photons, or uncontrolled degradation effects produced when the rupture electrical field of the metal oxide is overcome (see the Supporting Information). To exemplify the later point, it can be roughly estimated that nanowires contacted between two electrodes with a separation of only 50 nm[23] and polarized at 5 V [1,10] will be subjected to electrical fields as high as 1 MV/cm.

2.2. Intrinsic Properties of the Semiconductor. In addition to geometrical factors, the dependence of I_{ph} on intrinsic material properties, such as η , τ, μ^* and β , have to be considered (see eq 11). The spectral response of photodetectors is determined by the quantum efficiency η, which was observed to increase by up to 3 orders of magnitude when photons with energies above the bandgap interact with these devices, compared to typical responses obtained with sub-bandgap photons.[24] The variation of quantum efficiency η as a function of incident light wavelength (λ) was investigated. In Figure 7, it is demonstrated how I_{ph} scaled up when above-bandgap photons ($\lambda = 340 \pm 10$ nm) interacted with a single ZnO nanowire-based device, compared to low I_{ph} response obtained with sub-bandgap photons ($\lambda = 385 \pm 15$ nm). This result shows the importance of tuning the bandgap of such photodetectors to select their

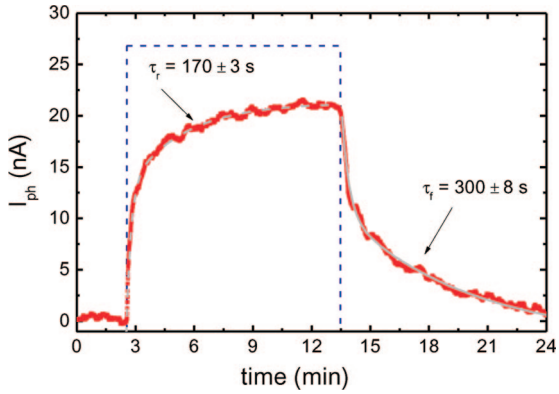

Figure 4. Dynamic behavior of the photoresponse I_{ph} measured with an individual ZnO nanowire when a UV pulse is applied (dashed line) ($\Phi_{ph} = 3.3 \times 10^{18}$ ph m^{-2} s^{-1}; $\lambda = 340 \pm 10$ nm; $V = 1$ V). The response fits with theoretically deduced exponential laws and exhibits time constants of $\tau_r = 170 \pm 3$ s and $\tau_d = 300 \pm 8$ s.

active/blind spectral regions.[11,18,24] It is noteworthy that the bandgap edge of nanowires depends not only on the material but also on their dimensions.[11,18] Thus, controlling the radii of nanowires is critical to tune the spectral sensitivity of the final devices.

The photogenerated carrier lifetime (τ) is the second parameter directly related to the intrinsic properties of nanowires, which is known to be higher in nanomaterials compared to bulk due to the large surface-to-volume ratio and the formation of deep level surface states.[18,25] For metal oxide nanowires, it is generally accepted that photocarrier relaxation dynamics consists of an initial decay process in the nanosecond range, explained by the fast carrier thermalization and hole-trapping by surface states, followed by a slow decay dependent on the surrounding atmosphere and the nanowire surface coating.[3,4,26,27] This second process, with characteristic time constants in seconds, dominates the final response of nanowire-based photodetectors. For this reason, the carrier lifetime contribution τ to the photoresponse I_{ph} (see eq 11) can be modified by controlling the surface interactions of this type of nanowires. Time-resolved measurements allowed us to estimate the rising time constant τ_r and falling time constant $\tau_d$exhibited by our devices (Figure 4). The evolution in time ($i_{ph}(t)$) was in accordance with the theoretical model (eqs 4 and 5), whereby values close to a few minutes were found.

The third parameter related to the intrinsic properties of nanowires is the electrical mobility μ^*, which is known to be dependent on their radii. In the case of ZnO, mobility values ranging from 2 to 30 cm^2/(V s) were reported for nanowires with radii below $r \approx 100$ nm.[28−31] The diminished mobility increases up to the bulk value (∼200 cm^2/(V s)) in thicker nanowires.[10] This behavior is attributed to scattering and trapping of the electrons by surface defect states and becomes more significant in thin nanowires possessing higher surface-to-volume ratios. Thus, thicker nanowires are convenient to obtain optimal devices for μ^* optimization due to minimized surface contributions μ_S (eq 7). The limitation introduced by the dependence of μ^* with radius can be also circumvented by passivating the nanowire surface, which is reported to dramatically increase the mobility of ZnO nanowires (up to 1.000 cm^2/(V s)).[31−34]

It was demonstrated that the mobility of ZnO nanowires dramatically increased (up to ∼1.000 cm^2/(V s)) with Si_3N_4/SiO_2,[31] polyimide,[32] poly(methyl methacrylate) (PMMA),[33] and polyacrylonitrile[34] coatings. Therefore, we covered some devices

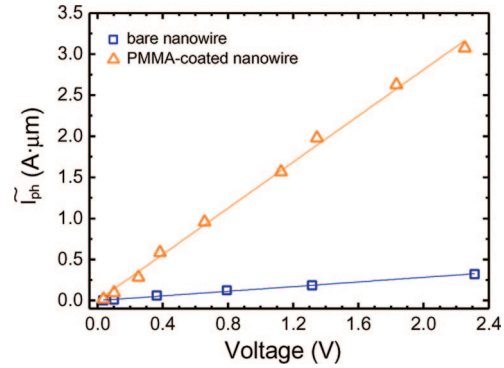

Figure 5. Photoresponse ($\tilde{I}_{ph} \equiv IL$) normalized to the distance between electrical contacts L of one single ZnO nanowire ($L_{NW} = 13$ μm) before and after coating with PMMA under identical illumination ($\Phi_{ph} = 3.3 \times 10^{18}$ ph m^{-2} s^{-1}; $\lambda = 340 \pm 10$ nm). $\tilde{I}_{ph}$ is higher after coating due to surface passivation induced higher μ^*.

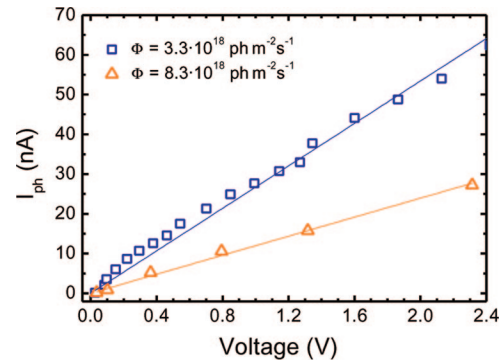

Figure 6. Linear dependency of photoresponses I_{ph} on the applied voltage V of an individual ZnO nanowire (under two different photon fluxes Φ_{ph}).

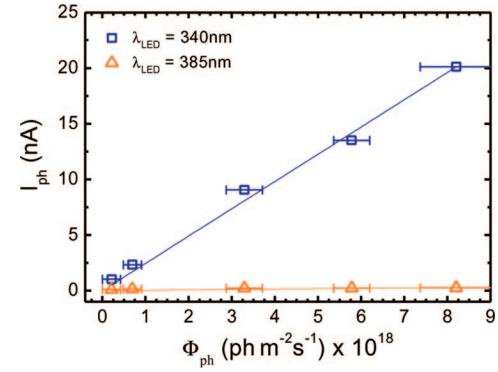

Figure 7. Photoresponse I_{ph} of an individual ZnO nanowire under different photon fluxes Φ_{ph} at constant polarization voltage ($V = 1$ V). A linear dependence between these two parameters is experimentally observed. Remarkably, photoresponse I_{ph} is highly dependent on the energy of the incident photons.

with PMMA by spin coating after eliminating the surface contamination with oxygen plasma. The passivation layers were approximately 500 nm thick, and presented high UV transparency (optical transmittance above 92% from 300 to 800 nm) and extremely low conductance (below 0.1 nS) independent of the illumination. The photoresponse of these devices was ∼9.5 times higher after coating (see Figure 5). To elucidate this point, the mobility of the nanowires[15] before and after passivation were estitmated to be $\mu^* \approx 3-5$ cm^2/(V s) and $\mu^*_{(PMMA)} \approx 40-53$ cm^2/(V s), respectively. This improvement in the nanowire mobility (factor of ∼10) and the high transmittance of the PMMA layer explain the increased photoresponse according to eq 11.

The last intrinsic parameter of nanowires to be considered in this work is the fraction of photons (β) not reflected by the surface of the metal oxide, which was recently demonstrated to be lower in photodetectors based on aligned nanowires compared to thin films.[35]

2.3. Working Conditions. As far as the experimental conditions are concerned, it can be expected from eqs 11 and 12 that photoresponse raises linearly with applied voltage V and flux of photons Φ_{ph}. Figures 6 and 7 demonstrate the linear increase in device response in dependence to the two parameters and UV-light according to theory. This feature complicates comparing most of the reported results, since different experimental conditions were used in these experiments.[1−10] For this reason we propose a more generic way to express eq 12,

$$g_{ph} \equiv \frac{L^2 G_{ph}}{V} \approx \eta \tau \mu^* \tag{14}$$

which is a normalized photoconductive gain, independent of the device geometry and the experimental conditions.

Apart from the photoconductive gain, the dynamic behavior of these devices is also important for optimizing real devices. Their low-pass bandwidth can be defined as $BW \approx (2\pi\tau)^{-1}$. Thus, the normalized gain per bandwidth becomes

$$g_{ph}BW \approx \frac{\eta \mu^*}{2\pi} \tag{15}$$

From equation 15, it can be observed that the quantum efficiency η and mobility μ^* are the key parameters to evaluate the overall performance of these photodetectors.

3. Comparison to State-of-the-art Devices. To substantiate and validate the performances of our nanowire-based devices, the photoresponse values were critically compared with previously reported results. Soci et al.[10] recently reported photoconductive gain values of $G_{ph,lit} = 5 \times 10^7$ in devices with $L_{lit} = 1\ \mu$m and $<r>_{lit} = 110$ nm polarized at $V_{lit} = 5$ V for equivalent illumination conditions, which is much higher than the typical G_{ph} values measured in our experiments. For example, $G_{ph} = 6 \times 10^3$ was obtained with $V = 1$ V, $L \approx 13\ \mu$m, and $r \approx 110$ nm. However, an accurate comparison of these two devices can be only achieved if the photoconductive gain G_{ph} is rewritten as shown in equation 14. If g_{ph} is calculated, we find that $g_{ph,lit} = 10^{-5}$ m^2/V and $g_{ph} = 10^{-6}$ m^2/V, showing that the literature value is only 1 order of magnitude higher than ours. This discrepancy can be explained considering the mobility μ^* and lifetime τ_d of nanowires. On one hand, our ZnO nanowires have response time constants close to $\tau \approx 300$s (Figure 4) and exhibited mobility values of $\sim$3 cm^2/(V s), which was estimated following a procedure described elsewhere.[15] On the other hand, Soci and co-workers reported $\tau_{lit} \approx 33$ s and $\mu^*_{lit} \approx 270$ cm^2/(V s), whose product ($\tau_{lit}\mu^*_{lit}$) is a factor 10 time higher than ours ($\tau\mu^*$), which justifies the divergence of values in g_{ph} (see eq 14). Fully consistent results were obtained with the rest of devices under test, demonstrating that gain normalization of photodetectors to the geometry and polarization conditions is necessary for adequate comparison. Moreover, comparison of g_{ph} values allows the determination of which intrinsic properties of the photoactive material must be improved to enhance the performance of future devices. For example, according to the experimental results, the electron mobility μ^* should be improved in our case. From all of these results, it can be concluded that the experimental responses obtained with photodetectors based on single nanowires are precisely modeled by the here-summarized theoretical approach.

Finally, the same methodology was applied to compare the photoresponse of ZnO nanowires and ZnO thin films.[36] In general, higher photocurrent values I_{ph} were obtained with larger grains,[37−41] due to increasing mobility which approaches bulk behavior ($\sim$200 cm^2/(V s)) in high-quality thin films,[42] with typical photoconductive gain values of $G^{TF}_{ph,lit} = 1360$.[38] Using the polarization and geometric conditions reported by the authors ($V^{TF}_{ph,lit} = 5$ V; $L^{TF}_{ph,lit} = 10\ \mu$), the normalized photoconductive gain was found to be $g^{TF}_{ph,lit} = 3 \times 10^{-8}$ m^2/V, whose value is clearly lower than the one reported with single ZnO nanowires. On the contrary, the normalized gain per bandwidth of ZnO thin films is significantly higher ($g^{TF}_{ph,lit}BW = 3 \times 10^{-3}$ m^2 Hz/V) than that obtained with ZnO nanowires ($g^{NW}_{ph,lit}BW = 5 \times 10^{-8}$ m^2 Hz/V[10]), if $\tau^{TF}_{lit} \approx 1.5\ \mu$s.[38] Comparing this result with eqs 14 and 15, it is concluded that the higher photogain achieved with individual nanowires is mainly associated to the longer lifetime of the photocarriers, which increases at the expense of diminishing dynamic response.

Conclusions

We presented in detail the principles ruling the response of UV photodetectors based on metal oxide nanowires. Different design and fabrication strategies to enhance their performances were identified and discussed, such as controlling their geometry or tuning the intrinsic electrical properties of nanowires. Most of them were validated with experimental results obtained with photodetectors based on single ZnO nanowires. Finally, a rigorous methodology to compare different devices was presented, overcoming the present lack of systematic study in this field. On the basis of this methodology we conclude that current photodetectors based on single ZnO nanowires achieve better normalized gains (up to 3 orders of magnitude) with slower response compared with thin film devices.

Acknowledgment. This work has been partially supported by the Spanish Ministry of Education (MEC) through the project N-MOSEN (MAT2007-66741-C02-01), the UE through the project NAWACS (NAN2006-28568-E), the Human Potential Program—Access to Research Infrastructures—, and the project MAGASENS and CROMINA. J.D.P. and R.J.D. are indebted to the MEC for the FPU grant. F.H.-R. is indebted to the MEC for the FPU grant and the support of the Torres Quevedo program (PTQ05-02-03201). Thanks are due to the German Science Foundation (DFG) for supporting this work in the frame of priority on nanomaterials—Sonderforschungsbereich 277—at the Saarland University, Saarbruecken, Germany.

Supporting Information Available: (I) Photogeneration theory details: nonuniform absorption and transient solution and (II) self-heating effects on nanowires. This information is available free of charge via the Internet at http://pubs.acs.org.

References and Notes

(1) Kind, H.; Yan, H.; Messer, B.; Law, M.; Yang, P. *Adv. Mater.* **2002**, *14*, 158–160.
(2) Keem, K.; Kim, H.; Kim, G. T.; Lee, J. S.; Min, B.; Cho, K.; Sung, M. Y.; Kim, S. *Appl. Phys. Lett.* **2004**, *84*, 4376–4378.
(3) Fan, Z. Y.; Chang, P. C.; Lu, J. G.; Walter, E. C.; Penner, R. M.; Lin, C. H.; Lee, H. P. *Appl. Phys. Lett.* **2004**, *85*, 6128–6130.
(4) Heo, Y. W.; Kang, B. S.; Tien, L. C.; Norton, D. P.; Ren, F.; La Roche, J. R.; Pearton, S. J. *Appl. Phys. A: Mater. Sci. Process.* **2005**, *80*, 497–499.
(5) Kumar, S.; Gupta, V.; Sreenivas, K. *Nanotechnology* **2005**, *16*, 1167–1171.
(6) Hsu, C. L.; Chang, S. J.; Lin, Y. R.; Li, P. C.; Lin, T. S.; Tsai, S. Y.; Lu, T. H.; Chen, I. C. *Chem. Phys. Lett.* **2005**, *416*, 75–78.
(7) Law, J. B. K.; Thong, J. T. L. *Appl. Phys. Lett.* **2006**, *88*, 133114.

(8) Luo, L.; Zhang, Y. F.; Mao, S. S.; Lin, L. W. *Sens. Actuators, A* **2006**, *127*, 201–206.

(9) Suehiro, J.; Nakagawa, N.; Hidaka, S.; Ueda, M.; Imasaka, K.; Higashihata, M.; Okada, T.; Hara, M. *Nanotechnology* **2006**, *17*, 2567–2573.

(10) Soci, C.; Zhang, A.; Xiang, B.; Dayeh, S. A.; Aplin, D. P. R.; Park, J.; Bao, X. Y.; Lo, Y. H.; Wang, D. *Nano Lett.* **2007**, *7*, 1003–1009.

(11) (a) Mathur, S.; Barth, S.; Shen, H.; Pyun, J. C.; Werner, U. *Small* **2005**, *1*, 713–717. (b) Mathur, S.; Barth, S. *Small* **2007**, *3*, 2070–2075.

(12) Wang, Z. L. *J. Phys.: Condens. Matter* **2004**, *16*, R829−R858.

(13) Hernández-Ramírez, F.; Rodríguez, J.; Casals, O.; Russinyol, E.; Vilà, A; Romano-Rodríguez, A.; Morante, J. R.; Abid, M. *Sens. Actuators, B* **2006**, *118*, 198–203.

(14) Hernández-Ramírez, F.; Tarancón, A.; Casals, O.; Rodríguez, J.; Romano-Rodríguez, A.; Morante, J. R.; Barth, S.; Mathur, S.; Choi, T. Y.; Poulikakos, D.; Callegari, V.; Nellen, P. M. *Nanotechnology* **2006**, *17*, 5577–5583.

(15) Hernandez-Ramirez, F.; Tarancon, A.; Casals, O.; Pellicer, E.; Rodriguez, J.; Romano-Rodriguez, A.; Morante, J. R.; Barth, S.; Mathur, S. *Phys. Rev. B* **2007**, *76*, 085429.

(16) Hernandez-Ramirez, F.; Prades, J. D.; Tarancon, A.; Barth, S.; Casals, O.; Jiménez-Diaz, R.; Pellicer, E.; Rodriguez, J.; Juli, M. A.; Romano-Rodriguez, A.; Morante, J. R.; Mathur, S.; Helwig, A.; Spannhake, J.; Mueller, G. *Nanotechnology* **2007**, *18*, 495501.

(17) Zhang, Z.; Yao, K.; Liu, Y.; Jin, C.; Liang, X.; Chen, Q.; Peng, L. M. *Adv. Funct. Mater.* **2007**, *17*, 2478–2489.

(18) (a) Rose, A. *Concepts in Photoconductivity and Allied Problems*; Interscience Publishers: New York, 1963. (b) Sze, S. M. *Physics of Semiconductor Devices*; John Wiley & Sons, Inc: New York, 1981. (c) Bube, R. H. *Photoelectronic Properties of Semiconductors*; Cambridge University Press: Cambridge, 1992.

(19) Yoshikawa, H.; Adachi, S. *Jpn. J. Appl. Phys* **1997**, *36*, 6237–6243.

(20) Wang, Z. L. *Mat. Today* **2004**, 26–33.

(21) Kumar, S.; Rajaraman, S.; Gerhardt, R. A.; Wang, Z. L.; Hesketh, P. J. *Electrochim. Acta* **2005**, *51*, 943–951.

(22) Suehiro, J.; Nakagawa, N.; Hidaka, S.; Ueda, M.; Imasaka, K.; Higashihata, M.; Okada, T.; Hara, M. *Nanotechnology* **2006**, *17*, 2567–2573.

(23) This resolution value was taken as a rough approximation to the minimal feature of current lithography techniques.

(24) Zheng, X. G.; Li, Q. Sh.; Zhao, J. P.; Chen, D.; Zhao, B.; Yang, Y. J.; Zhang, L. Ch. *Appl. Surf. Sci.* **2006**, *253*, 2264–2267.

(25) Jie, J. S.; Zhang, W. J.; Jiang, Y.; Meng, X. M.; Li, Y. Q.; Lee, S. T. *Nano Lett.* **2006**, *6*, 1887–1892.

(26) Studenikin, S. A.; Golego, N.; Cocivera, M. *J. Appl. Phys.* **2000**, *87*, 2413–2421.

(27) Lao, C. S.; Park, M. C.; Kuang, Q.; Deng, Y.; Sood, A. K.; Polla, D. L.; Wang, Z. L. *J. Am. Chem. Soc.* **2007**, *129*, 12096–12097.

(28) Chang, P. C.; Chien, C. J.; Stichtenoth, D.; Ronning, C.; Lu, J. G. *Appl. Phys. Lett.* **2007**, *90*, 113101.

(29) Fan, Z. Y.; Wang, D. W.; Chang, P. C.; Tseng, W. Y.; Lu, J. G. *Appl. Phys. Lett.* **2004**, *85*, 5923.

(30) Chang, P. C.; Fan, Z.; Wang, D.; Tseng, W. Y.; Chiou, W. A.; Hong, J.; Lu, J. G. *Chem. Mater.* **2004**, *16*, 5133–5137.

(31) Chang, P.; Fan, Z.; Chien, C.; Stichtenoth, D.; Ronning, C.; Lu, J. G. *Appl. Phys. Lett.* **2006**, *89*, 133113.

(32) Park, W. I.; Kim, J. S.; Yi, G.-C.; Bae, M. H.; Lee, H.-J. *Appl. Phys. Lett.* **2004**, *85*, 5052–5054.

(33) Hong, W.-K.; Kimm, B.-J.; Kim, T.-W.; Jo, G.; Song, S.; Kwon, S.-S.; Yoon, A.; Stach, E. A.; Lee, T. *Colloids Surf. A* **2008**, *313−314*, 378–382.

(34) He, J. H.; Lin, Y. H.; McConney, M. E.; Tsuruk, V. V.; Wang, Z. L.; Bao, G. *J. Appl. Phys.* **2007**, *102*, 084303.

(35) Hu, L.; Chen, G. *Nano Lett.* **2007**, *7*, 3249–3252.

(36) Monroy, E.; Omnes, F.; Calle, F. *Semicond. Sci. Technol.* **2003**, *18*, R33−R51.

(37) Takahashi, Y.; Kanamori, M.; Kondoh, A.; Minoura, H.; Ohya, Y *Jpn. J. Appl. Phys* **1994**, *33*, 6611–6615.

(38) Liu, Y.; Gorla, C. R.; Liang, S.; Emanetoglu, N.; Lu, Y.; Shen, H.; Wraback, M. *J. Electron. Mater.* **2000**, 29.

(39) Basak, D.; Amin, G.; Mallik, B.; Paul, G. K.; Sen, S. K. *J. Cryst. Growth* **2003**, *256*, 73–77.

(40) Liu, M.; Kim, H. K. *Appl. Phys. Lett.* **2004**, *84*, 173–175.

(41) Liu, J.; Xia, Y.; Wang, L.; Su, Q.; Shi, W. *Appl. Surf. Sci.* **2006**, *253*, 5218–5222.

(42) Ohtomo, A.; Tsukazaki, A. *Semicond. Sci. Technol.* **2005**, *20*, S1−S12.

JP804614Q